Breathing lessons for PET/CT: Bacharach looks at the trade-offs in switching from stand-alone PET to PET/CT and previews 3 articles in this month's *JNM* that focus on various challenges of CT-based attenuation correction. . . . . ***Page 677***

Characterizing pulmonary hypertension: Tunariu and colleagues compare the efficacy of ventilation–perfusion scintigraphy with that of CT pulmonary angiography in identifying patients with chronic thromboembolic pulmonary disease and in hastening the initiation of effective therapies. . . ***Page 680***

Posthepatectomy liver failure risk: Dinant and colleagues compare the abilities of preoperative hepatobiliary scintigraphy and CT volumetric measurement of future remnant liver to predict postoperative morbidity, organ failure, and mortality in patients undergoing liver resection. . . . . ***Page 685***

Tracer influence on lymphoscintigraphy: Bourgeois evaluates whether and how the volume and quantity of injected ^{99m}Tc-labeled colloids—data usually not included in scientific reports—affect lymphoscintigraphic results. . . . . ***Page 693***

Cardiac SPECT/CT fusion: Gaemperli and colleagues report on initial experience with fused 3D SPECT/CT in patients with coronary artery disease and on the potential of this technique for providing incremental diagnostic information on the functional relevance of coronary artery lesions. . . ***Page 696***

PET and MRI in mild dementia: Ishii and colleagues investigate regional and pathophysiologic differences in morphologic and functional changes in patients with mild dementia with Lewy bodies and individuals with very early Alzheimer's disease. . . . . ***Page 704***

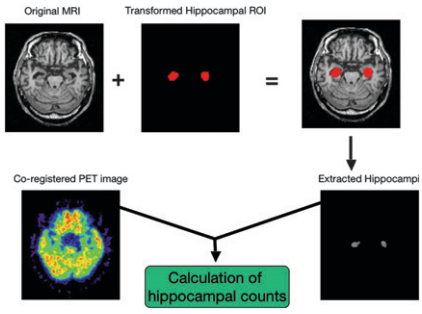

Deep breath-hold PET/CT: Meirelles and colleagues detail the detection and characterization of thoracic lesions by PET/CT imaging acquired with and without a novel deep-inspiration protocol. . . . . ***Page 712***

^{18}F-TYR PET/CT and meningiomas: Rutten and colleagues describe results with PET/CT and 2-^{18}F-fluoro-l-tyrosine, a marker of amino acid transport, as part of routine yearly follow-up of patients previously irradiated for skull base meningiomas. . . . . ***Page 720***

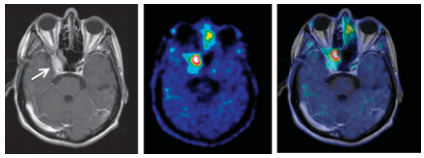

^{18}F-FLT PET in lymph node staging: Troost and colleagues assess the value of ^{18}F-FLT PET in determining lymph node status in patients with newly diagnosed squamous cell carcinoma of the head and neck. . . ***Page 726***

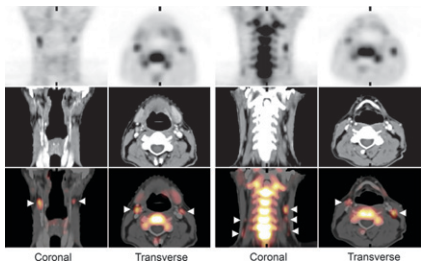

GLP-1 receptors in tumors: Körner and colleagues report on in vitro evaluations of GLP-1 receptor expression in a variety of human tumors and nonneoplastic tissues and discuss the promise of GLP-1 receptors in molecular scintigraphy and targeted radiotherapy. . . . . ***Page 736***

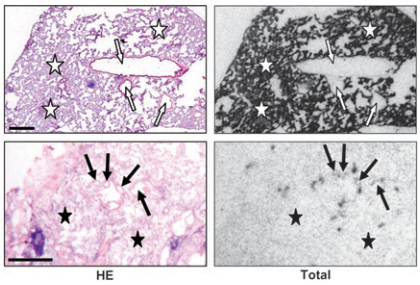

PET predictions in NSCLC: Nahmias and colleagues describe patient studies assessing the ability of ^{18}F-FDG PET to characterize early metabolic response to chemotherapy in patients with non–small cell lung cancer and to predict therapeutic success or failure. . . . . ***Page 744***

PET and treatment prognosis: Kim and colleagues evaluate the effectiveness of pretreatment ^{18}F-FDG PET in providing guidance for choice of initial treatment in patients with squamous cell carcinoma of the oropharynx. . . . . ***Page 752***

Postacquisition motion detection in PET: Bundschuh and colleagues report on the feasibility of a technique using list-mode data to detect craniocaudal movement of thoracic and abdominal lesions in PET imaging without an external gating device. . . . . ***Page 758***

Delayed PET/CT in bladder cancer: Anjos and colleagues investigate the role of delayed ^{18}F-FDG PET/CT in the detection and restaging of bladder cancer, using a diuretic and oral hydration to remove excreted tracer from the bladder. . . . . ***Page 764***

PET and molecular markers: Riedl and colleagues explore the prognostic capabilities of PET by determining the extent to which presurgical ^{18}F-FDG PET images in metastatic colorectal cancer correlate with

other cellular characteristics and clinical behaviors of these tumors. . . . ***Page 771***

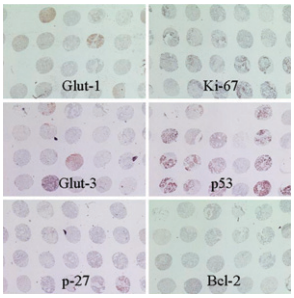

Metabolic asymmetry in epilepsy: Lin and colleagues describe an approach to identify and quantify those aspects of metabolic asymmetry in presurgical PET scans that may accurately predict postsurgical seizure-free clinical outcomes in patients with temporal lobe epilepsy. . . . . ***Page 776***

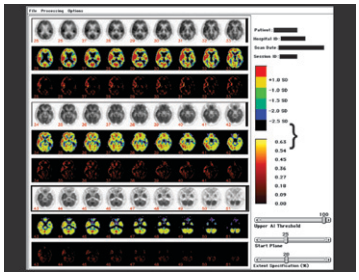

Cardiac PET/CT imaging: Di Carli and colleagues provide an educational overview of the advantages and challenges of myocardial perfusion PET and integrated PET/CT, with a focus on the hybrid technology's potential for translating advances in molecularly targeted imaging to humans. . . . . ***Page 783***

Cine CT in cardiac PET/CT: Alessio and colleagues investigate the use of cine CT, acquiring multiple low-dose CT images during a respiratory cycle, as an alternative to helical CT in cardiac PET attenuation correction. . . . . ***Page 794***

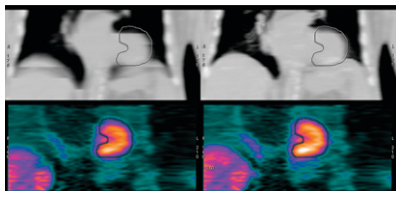

Iterative partial-volume correction: Teo and colleagues describe an iterative postreconstruction method that corrects for partial-volume errors in PET, thereby enhancing the accuracy of radiopharmaceutical uptake estimates in small tumors. . . . . ***Page 802***

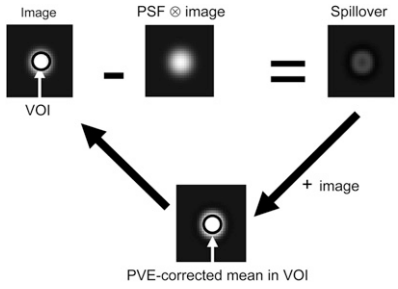

CT-corrected canine cardiac PET: Cook and colleagues compare respiration-averaged CT and 4D CT for attenuation correction of cardiac PET in an in vivo canine model. . . . . ***Page 811***

Human-derived PET reporter gene: Ponomarev and colleagues describe preliminary assessment of a human-derived intrinsically nonimmunogenic reporter gene for PET imaging of molecular–genetic processes and discuss potential clinical applications. . . . . ***Page 819***

^{124}I-MIBG hNET reporter gene imaging: Moroz and colleagues detail the construction of a novel internal ribosomal entry site–linked norepinephrine transporter hybrid reporter gene radiolabeled for both nuclear and optical imaging. . . . ***Page 827***

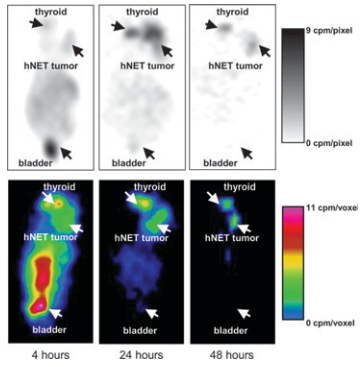

Quantitative PET with microfluidics: Wu and colleagues describe an automated blood sampling device on an integrated microfluidic platform for precise small-quantity blood withdrawal in PET studies of mice. . . . . ***Page 837***

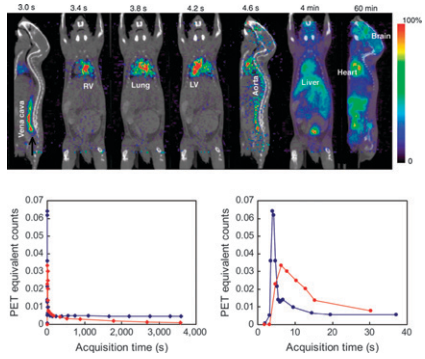

ON THE COVER

At top left, perfusion polar maps at stress and rest show a largely reversible anteroapical perfusion defect (arrowhead). At top right, 3-dimensional volume-rendered CT angiogram shows the coronary vessel tree with stenosis of the mid left anterior descending artery (LAD) and proximal stenosis of the first diagonal branch (DA1). At bottom left, fused 3-dimensional SPECT/CT image shows that the DA1 stenosis is the functionally relevant lesion. At bottom right, findings are confirmed by invasive coronary angiography.

SEE PAGE 701